# Defective cholesterol clearance limits remyelination in the aged central nervous system

**Ludovico Cantuti-Castelvetri,[1,2,3,4]\* Dirk Fitzner,[1,5]\* Mar Bosch-Queralt,[1,2,3,4] Marie-Theres Weil,[1,6] Minhui Su,[1,2,3,4] Paromita Sen,[1] Torben Ruhwedel,[7] Miso Mitkovski,[8] George Trendelenburg,[5] Dieter Lütjohann,[9] Wiebke Möbius,[6,7] Mikael Simons[1,2,3,4]†**

[1]Max Planck Institute of Experimental Medicine, 37075 Göttingen, Germany. [2]Munich Cluster for Systems Neurology (SyNergy), 81377 Munich, Germany. [3]Institute of Neuronal Cell Biology, Technical University Munich, 80805 Munich, Germany. [4]German Center for Neurodegenerative Disease (DZNE), 81377 Munich, Germany. [5]Department of Neurology, University of Göttingen Medical Center, 37075 Göttingen, Germany. [6]Center Nanoscale Microscopy and Molecular Physiology of the Brain (CNMPB), 37075 Göttingen, Germany. [7]Department of Neurogenetics, Max Planck Institute of Experimental Medicine, 37075 Göttingen, Germany. [8]Light Microscopy Facility, Max Planck Institute of Experimental Medicine, 37075 Göttingen Germany. [9]Institute for Clinical Chemistry and Clinical Pharmacology, University of Bonn, 53127 Bonn, Germany.

\*These authors contributed equally to this work.

†Corresponding author. Email: msimons@gwdg.de

**Age-associated decline in regeneration capacity limits the restoration of nervous system functionality after injury. In a model for demyelination, we found that old mice fail to resolve the inflammatory response initiated after myelin damage. Aged phagocytes accumulated excessive amounts of myelin debris, which triggered cholesterol crystal formation, phagolysosomal membrane rupture, and stimulated inflammasomes. Myelin debris clearance required cholesterol transporters including apolipoprotein E. Remarkably, stimulation of reverse cholesterol transport was sufficient to restore the capacity of old mice to remyelinate lesioned tissue. Thus, cholesterol-rich myelin debris can overwhelm the efflux capacity of phagocytes, resulting in a phase transition of cholesterol into crystals thereby inducing a maladaptive immune response that impedes tissue regeneration.**

Remyelination restores rapid transmission of nerve impulses and axonal function in the CNS of patients with demyelinating diseases such as multiple sclerosis (MS). Although remyelination can occur in MS, age-associated decline in myelin repair contributes to chronic progressive disease and disability (*1*). Thus, understanding the cause of and preventing this decline is a key goal in regenerative medicine (*2–4*). So far, epigenetic changes within aging oligodendrocyte progenitor cells and declines in phagocytic capacity of aged blood-derived monocytes have been identified as possible mechanisms (*5, 6*). We implemented a toxin-induced model, in which a single injection of lysolecithin (lysophosphatidylcholine) induces a focal demyelinating lesion in the white matter of the brain or spinal cord of mice. In lesioned animals, demyelination is complete within 4 days, followed by a repair process that is maximal between 14 to 21 days post injection (dpi) and requires rapid clearance of damaged myelin for regeneration to occur (*7*). We induced focal demyelinating lesions in the corpus callosum of young (3 months) and old (12 months) mice by lysolecithin injections. Lesions were of similar size at 4 dpi, but not at 14 dpi confirming the poor regenerative capacity of old mice (Fig. 1, A to C, and fig. S1, A to E). Sustained immune infiltration, as determined by IBA1-positive and MAC2-positive cells, was detected in old mice at 14dpi (Fig. 1, A and E, and fig. S1G). Myelin debris accumulation within lysosomes of phagocytes (Fig. 1, D and F) and numerous foam cells harboring lipid droplets and needle-shaped cholesterol crystals - a typical hallmark of cholesterol overloading - were found in old mice (Fig. 1, G and H, and fig. S2G). Moreover, by a combination of laser reflection and fluorescence confocal microscopy (reflection microscopy) we confirmed the increase of crystal deposition in spinal cord lesions of old mice (Fig. 1, I and J). Crystals were similarly observed in two other models of myelin injury (fig. S2).

Toxic overload of cholesterol drives the formation of foamy macrophages and maladaptive immune responses in atherosclerosis. We hypothesized that the accumulation of cholesterol, the major component of myelin, may overwhelm the cholesterol transport capacity of phagocytes, thereby forming a bottleneck for successful repair in the aged CNS. Because cholesterol cannot be broken down it needs to be transferred from the phagocytes back to the extracellular space using the transporters ATP-Binding Cassette A1 and G1 (ABCA1 and ABCG1) in the plasma membrane where it binds high-density lipoprotein particles (e.g., APOE) (*8*). Real-time quantitative reverse transcription PCR revealed that the expression of *ApoE*, *Abca1* and *Abcg1*, was reduced in 4 dpi lesions of old compared to young mice (Fig. 1, K to M, and fig. S3). Oxysterols (hydroxylated cholesterol metabolites) such

as 24S- and 27-hydroxycholesterol are endogenous ligands for liver X receptor (LXR), thereby controlling the expression of genes involved in cholesterol efflux in cholesterol-loaded cells (*9*). Relative amounts of 24S-hydroxycholesterol did not differ in lesions of young and old animals, but 27-hydroxycholesterol levels were reduced in lesions of old mice (fig. S3). One possible explanation for lesion restitution failure in old mice is the inability to clear excessive myelin-derived cholesterol from phagocytes. Thus, we examined whether the LXR agonist, GW3965 (*10*) improve lesion recovery in old mice by inducing the expression of genes involved in lipid efflux, such as *Abca1*, *Abcg1* and *ApoE* (fig. S3). GW3965 led to markedly improved lesion regeneration in old mice with a reduction in the number of IBA1-positive and MAC2-positive phagocytes (Fig. 1, A to C). In addition, the number of phagocytes containing myelin debris, the number of foam cells and the amount of cholesterol crystals was reduced by treatment with GW3965 (Fig. 1, A to J).

Because accumulation of cholesterol in phagocytes may pose a barrier for successful tissue regeneration, we analyzed the regenerative capacity of mouse mutants lacking central factors of the reverse cholesterol transport pathway. We induced demyelinating lesions in 3 month old NR1H3 (or LXRα) knockout mice and observed, as in aged wild-type mice, impaired lesion restitution and sustained phagocyte infiltration at 21 dpi (fig. S4, A to C). In addition, we detected accumulation of myelin debris in lysosomes of phagocytes and crystal deposition in lesions of LXRα KO mice (fig. S4, D to G).

Next, we analyzed the role of apolipoprotein E (APOE), the major CNS cholesterol carrier that supports lipid efflux from cells (*11*). We induced focal demyelination in the corpus callosum of 12-week old APOE knockout (APOE KO) and wild-type control mice and quantified lesion size and recovery. Lesion size did not differ initially, at 4 dpi (fig. S4, H to J). However, when lesions were analyzed at 21 dpi, we observed impaired lesion restitution. We detected an increased number of IBA1-positive, MAC2-positive and MHCII-positive phagocytes, crystal deposition and myelin debris accumulation within lysosomes of phagocytes in spinal cord and corpus callosum lesions of APOE KO animals as compared to control mice (Fig. 2 and fig. S5). Because APOE has functions beyond cholesterol transport (*11*), we tested the efficacy of cyclic oligosaccharide 2-hydroxypropyl-β-cyclodextrin (HβCD), a compound that increases cholesterol efflux and solubility (*12*); and found that HβCD treatment attenuated the phenotype of APOE KO animals (Fig. 3 and fig. S6).

*ApoE* represents together with *Abca1* and *Abcg1* the major nuclear liver X receptor regulated genes that are involved in mediating cholesterol efflux from phagocytes. We thus crossbred CX3CR1CreER animals with Abca1$^{fl/fl}$ and Abcg1$^{fl/fl}$ mice to obtain microglia/macrophage specific double knockout

mice (ABCA1/G1 KO). We observed an increased number of IBA1-positive and MHCII-positive phagocytes, an increase in crystal deposition and fewer myelinated axons in 21 dpi lesions of ABCA1/G1 KO animals as compared to control (fig. S7).

Because excessive cholesterol accumulation in phagocytes limits lesion recovery, we turned to cell culture experiments to determine the mechanisms involved. We prepared phagocytes (primary microglia or bone marrow-derived macrophages) from APOE KO and wild-type mice and examined the phagocytic uptake of myelin debris, which did not differ in cells prepared from wild-type or APOE KO mice (fig. S8, A and B). Because APOE is also produced by astrocytes, we incubated cells in the presence of serum-free conditioned media prepared from either wild-type or APOE KO astrocytes and observed the clearance of the internalized myelin particles from phagocytes. Myelin debris persisted within lysosomes of APOE KO cells that were incubated with conditioned media from APOE KO astrocytes. Clearance could be improved by an APOE-derived mimetic peptide, ATI5261 (*13*), which contains an amphipathic α-helical motif responsible for lipid binding and cholesterol efflux (Fig. 3, E and F). Moreover, myelin debris treatment resulted in crystal formation, which was increased in APOE KO macrophages and reduced by GW3965 treatment (fig. S8, C to G).

In atherosclerosis, cholesterol crystals can induce inflammation by phagolysosomal membrane rupture and subsequent stimulation of the caspase-1-activating NLRP3 (NALP3 or cryopyrin) inflammasome and secretion of interleukin (IL)-1 cytokines (*14*, *15*). Myelin debris treatment resulted in lysosomal permeabilization and caspase-1 cleavage in wild-type, but not in NLRP3-deficient macrophages (Fig. 4, A to H, and fig. S9, A and B). More pronounced caspase-1 activation was observed in APOE KO as compared to wild-type macrophages, which was confirmed in vivo in APOE KO mice after lysolecithin injection (Fig. 4E and fig. S9C). Myelin overloading induced cell death, which resulted in DNA fragmentation (detected by TUNEL assay), was cholesterol-dependent (fig. S9, D and E), and rescued by caspase-1 inhibitors pointing to an inflammasome-mediated pyroptotic cell death pathway (Fig. 4G and fig. S10). Thus, cholesterol derived from myelin debris can activate the NLRP3 inflammasome in macrophages when toxic levels build up intracellularly in the absence of sufficient lipoprotein carriers.

Because jamming the lysosomal system with myelin debris resulted in cholesterol crystallization and inflammasome activation, we asked whether this pathway was responsible for limiting regeneration in old mice. To examine whether increased inflammasome activation contributed to the poor recovery of old mice, we analyzed spinal cord lesions of aged wild-type and NLRP3-deficient mice. As in GW3965 treated old animals (Fig. 4, I and J), we found significantly improved

remyelination in aged NLRP3-deficient mice as compared to aged wild-type mice at 21 dpi. Thus, inflammasome activation possibly downstream of cholesterol accumulation drives a maladaptive immune response impairing inflammation resolution and repair in aged mice.

Self-resolving inflammation is essential for a proper restorative process after tissue damage, while uncontrolled inflammation can leave lasting marks that permanently alter tissue homeostasis (*16*). Here, we made the surprising finding that the self-limiting inflammatory response, which is necessary to initiate a regenerative process, is maladaptive in the CNS of aged mice. It appears that the inability of aged phagocytes to clear the enormous amounts of cholesterol that are released from myelin after myelin breakdown in demyelinating diseases results in a phase transition of free cholesterol into crystals, inducing lysosomal rupture and inflammasome stimulation, which is consistent with the beneficial effects of nuclear receptor agonists in remyelination (*17*, *18*). The unexpected link between lipid metabolisms and tissue regeneration provides opportunities for the development of regenerative medicines for remyelination and for improving functional recovery after CNS injury (*19*).

## REFERENCES AND NOTES

1. P. Patrikios, C. Stadelmann, A. Kutzelnigg, H. Rauschka, M. Schmidbauer, H. Laursen, P. S. Sorensen, W. Brück, C. Lucchinetti, H. Lassmann, Remyelination is extensive in a subset of multiple sclerosis patients. *Brain* 129, 3165–3172 (2006). doi:10.1093/brain/awl217 Medline
2. F. J. Najm, M. Madhavan, A. Zaremba, E. Shick, R. T. Karl, D. C. Factor, T. E. Miller, Z. S. Nevin, C. Kantor, A. Sargent, K. L. Quick, D. M. Schlatzer, H. Tang, R. Papoian, K. R. Brimacombe, M. Shen, M. B. Boxer, A. Jadhav, A. P. Robinson, J. R. Podojil, S. D. Miller, R. H. Miller, P. J. Tesar, Drug-based modulation of endogenous stem cells promotes functional remyelination in vivo. *Nature* 522, 216–220 (2015). doi:10.1038/nature14335 Medline
3. F. Mei, S. P. J. Fancy, Y.-A. A. Shen, J. Niu, C. Zhao, B. Presley, E. Miao, S. Lee, S. R. Mayoral, S. A. Redmond, A. Etxeberria, L. Xiao, R. J. M. Franklin, A. Green, S. L. Hauser, J. R. Chan, Micropillar arrays as a high-throughput screening platform for therapeutics in multiple sclerosis. *Nat. Med.* 20, 954–960 (2014). doi:10.1038/nm.3618 Medline
4. V. A. Deshmukh, V. Tardif, C. A. Lyssiotis, C. C. Green, B. Kerman, H. J. Kim, K. Padmanabhan, J. G. Swoboda, I. Ahmad, T. Kondo, F. H. Gage, A. N. Theofilopoulos, B. R. Lawson, P. G. Schultz, L. L. Lairson, A regenerative approach to the treatment of multiple sclerosis. *Nature* 502, 327–332 (2013). doi:10.1038/nature12647 Medline
5. J. M. Ruckh, J.-W. Zhao, J. L. Shadrach, P. van Wijngaarden, T. N. Rao, A. J. Wagers, R. J. M. Franklin, Rejuvenation of regeneration in the aging central nervous system. *Cell Stem Cell* 10, 96–103 (2012). doi:10.1016/j.stem.2011.11.019 Medline
6. S. Shen, J. Sandoval, V. A. Swiss, J. Li, J. Dupree, R. J. M. Franklin, P. Casaccia-Bonnefil, Age-dependent epigenetic control of differentiation inhibitors is critical for remyelination efficiency. *Nat. Neurosci.* 11, 1024–1034 (2008). doi:10.1038/nn.2172 Medline
7. V. E. Miron, A. Boyd, J.-W. Zhao, T. J. Yuen, J. M. Ruckh, J. L. Shadrach, P. van Wijngaarden, A. J. Wagers, A. Williams, R. J. M. Franklin, C. Ffrench-Constant, M2 microglia and macrophages drive oligodendrocyte differentiation during CNS remyelination. *Nat. Neurosci.* 16, 1211–1218 (2013). doi:10.1038/nn.3469 Medline
8. K. J. Moore, I. Tabas, Macrophages in the pathogenesis of atherosclerosis. *Cell* 145, 341–355 (2011). doi:10.1016/j.cell.2011.04.005 Medline
9. X. Fu, J. G. Menke, Y. Chen, G. Zhou, K. L. MacNaul, S. D. Wright, C. P. Sparrow, E. G. Lund, 27-hydroxycholesterol is an endogenous ligand for liver X receptor in cholesterol-loaded cells. *J. Biol. Chem.* 276, 38378–38387 (2001).
doi:10.1074/jbc.M105805200 Medline
10. C. Hong, P. Tontonoz, Liver X receptors in lipid metabolism: Opportunities for drug discovery. *Nat. Rev. Drug Discov.* 13, 433–444 (2014). doi:10.1038/nrd4280 Medline
11. R. W. Mahley, Apolipoprotein E: Cholesterol transport protein with expanding role in cell biology. *Science* 240, 622–630 (1988). doi:10.1126/science.3283935 Medline
12. S. Zimmer, A. Grebe, S. S. Bakke, N. Bode, B. Halvorsen, T. Ulas, M. Skjelland, D. De Nardo, L. I. Labzin, A. Kerksiek, C. Hempel, M. T. Heneka, V. Hawxhurst, M. L. Fitzgerald, J. Trebicka, I. Björkhem, J.-A. Gustafsson, M. Westerterp, A. R. Tall, S. D. Wright, T. Espevik, J. L. Schultze, G. Nickenig, D. Lütjohann, E. Latz, Cyclodextrin promotes atherosclerosis regression via macrophage reprogramming. *Sci. Transl. Med.* 8, 333ra50 (2016). doi:10.1126/scitranslmed.aad6100 Medline
13. A. Hafiane, J. K. Bielicki, J. O. Johansson, J. Genest, Apolipoprotein E derived HDL mimetic peptide ATI-5261 promotes nascent HDL formation and reverse cholesterol transport in vitro. *Biochim. Biophys. Acta* 1841, 1498–1512 (2014). doi:10.1016/j.bbalip.2014.07.018 Medline
14. P. Duewell, H. Kono, K. J. Rayner, C. M. Sirois, G. Vladimer, F. G. Bauernfeind, G. S. Abela, L. Franchi, G. Nuñez, M. Schnurr, T. Espevik, E. Lien, K. A. Fitzgerald, K. L. Rock, K. J. Moore, S. D. Wright, V. Hornung, E. Latz, NLRP3 inflammasomes are required for atherogenesis and activated by cholesterol crystals. *Nature* 464, 1357–1361 (2010). doi:10.1038/nature08938 Medline
15. K. Rajamäki, J. Lappalainen, K. Oörni, E. Välimäki, S. Matikainen, P. T. Kovanen, K. K. Eklund, Cholesterol crystals activate the NLRP3 inflammasome in human macrophages: A novel link between cholesterol metabolism and inflammation. *PLOS ONE* 5, e11765 (2010). doi:10.1371/journal.pone.0011765 Medline
16. A. Aguzzi, B. A. Barres, M. L. Bennett, Microglia: Scapegoat, saboteur, or something else? *Science* 339, 156–161 (2013). doi:10.1126/science.1227901 Medline
17. J. K. Huang, A. A. Jarjour, B. N. Oumesmar, C. Kerninon, A. Williams, W. Krezel, H. Kagechika, J. Bauer, C. Zhao, A. Baron-Van Evercooren, P. Chambon, C. Ffrench-Constant, R. J. M. Franklin, Retinoid X receptor gamma signaling accelerates CNS remyelination. *Nat. Neurosci.* 14, 45–53 (2011). doi:10.1038/nn.2702 Medline
18. D. Meffre, G. Shackleford, M. Hichor, V. Gorgievski, E. T. Tzavara, A. Trousson, A. M. Ghoumari, C. Deboux, B. Nait Oumesmar, P. Liere, M. Schumacher, E.-E. Baulieu, F. Charbonnier, J. Grenier, C. Massaad, Liver X receptors alpha and beta promote myelination and remyelination in the cerebellum. *Proc. Natl. Acad. Sci. U.S.A.* 112, 7587–7592 (2015). doi:10.1073/pnas.1424951112 Medline
19. F. Bei, H. H. C. Lee, X. Liu, G. Gunner, H. Jin, L. Ma, C. Wang, L. Hou, T. K. Hensch, E. Frank, J. R. Sanes, C. Chen, M. Fagiolini, Z. He, Restoration of visual function by enhancing conduction in regenerated axons. *Cell* 164, 219–232 (2016). doi:10.1016/j.cell.2015.11.036 Medline
20. J. A. Piedrahita, S. H. Zhang, J. R. Hagaman, P. M. Oliver, N. Maeda, Generation of mice carrying a mutant apolipoprotein E gene inactivated by gene targeting in embryonic stem cells. *Proc. Natl. Acad. Sci. U.S.A.* 89, 4471–4475 (1992). doi:10.1073/pnas.89.10.4471 Medline
21. G. Liang, J. Yang, J. D. Horton, R. E. Hammer, J. L. Goldstein, M. S. Brown, Diminished hepatic response to fasting/refeeding and liver X receptor agonists in mice with selective deficiency of sterol regulatory element-binding protein-1c. *J. Biol. Chem.* 277, 9520–9528 (2002). doi:10.1074/jbc.M111421200 Medline
22. M. Westerterp, S. Gourion-Arsiquaud, A. J. Murphy, A. Shih, S. Cremers, R. L. Levine, A. R. Tall, L. Yvan-Charvet, Regulation of hematopoietic stem and progenitor cell mobilization by cholesterol efflux pathways. *Cell Stem Cell* 11, 195–206 (2012). doi:10.1016/j.stem.2012.04.024 Medline
23. S. Yona, K.-W. Kim, Y. Wolf, A. Mildner, D. Varol, M. Breker, D. Strauss-Ayali, S. Viukov, M. Guilliams, A. Misharin, D. A. Hume, H. Perlman, B. Malissen, E. Zelzer, S. Jung, Fate mapping reveals origins and dynamics of monocytes and tissue macrophages under homeostasis. *Immunity* 38, 79–91 (2013). doi:10.1016/j.immuni.2012.12.001 Medline
24. S. Safaiyan, N. Kannaiyan, N. Snaidero, S. Brioschi, K. Biber, S. Yona, A. L. Edinger, S. Jung, M. J. Rossner, M. Simons, Age-related myelin degradation burdens the clearance function of microglia during aging. *Nat. Neurosci.* 19, 995–998 (2016). doi:10.1038/nn.4325 Medline
25. E. O. Samstad, N. Niyonzima, S. Nymo, M. H. Aune, L. Ryan, S. S. Bakke, K. T.

Lappegård, O.-L. Brekke, J. D. Lambris, J. K. Damås, E. Latz, T. E. Mollnes, T. Espevik, Cholesterol crystals induce complement-dependent inflammasome activation and cytokine release. *J. Immunol.* **192**, 2837–2845 (2014). doi:10.4049/jimmunol.1302484 Medline

26. C. Oberle, J. Huai, T. Reinheckel, M. Tacke, M. Rassner, P. G. Ekert, J. Buellesbach, C. Borner, Lysosomal membrane permeabilization and cathepsin release is a Bax/Bak-dependent, amplifying event of apoptosis in fibroblasts and monocytes. *Cell Death Differ.* **17**, 1167–1178 (2010). doi:10.1038/cdd.2009.214 Medline

27. N. Snaidero, W. Möbius, T. Czopka, L. H. P. Hekking, C. Mathisen, D. Verkleij, S. Goebbels, J. Edgar, D. Merkler, D. A. Lyons, K.-A. Nave, M. Simons, Myelin membrane wrapping of CNS axons by PI(3,4,5)P3-dependent polarized growth at the inner tongue. *Cell* **156**, 277–290 (2014). doi:10.1016/j.cell.2013.11.044 Medline

28. D. Lütjohann, C. Hahn, W. Prange, T. Sudhop, M. Axelson, T. Sauerbruch, K. von Bergmann, C. Reichel, Influence of rifampin on serum markers of cholesterol and bile acid synthesis in men. *Int. J. Clin. Pharmacol. Ther.* **42**, 307–313 (2004). doi:10.5414/CPP42307 Medline

29. K. M. Thelen, K. M. Rentsch, U. Gutteck, M. Heverin, M. Olin, U. Andersson, A. von Eckardstein, I. Björkhem, D. Lütjohann, Brain cholesterol synthesis in mice is affected by high dose of simvastatin but not of pravastatin. *J. Pharmacol. Exp. Ther.* **316**, 1146–1152 (2006). doi:10.1124/jpet.105.094136 Medline

## ACKNOWLEDGMENTS

## SUPPLEMENTARY MATERIALS

www.sciencemag.org/cgi/content/full/science.aan4183/DC1
Materials and Methods
Figs. S1 to S10
References (*20–29*)
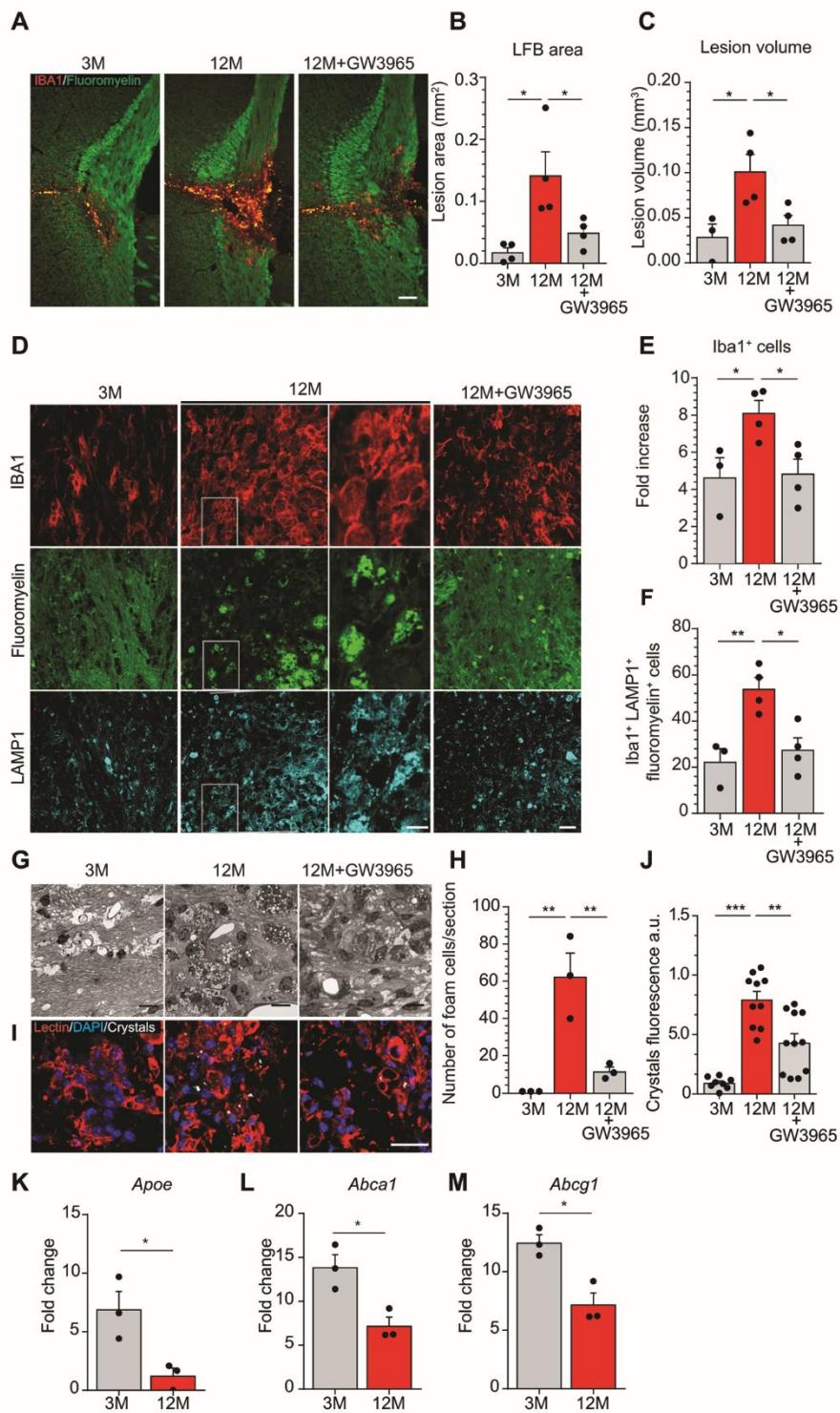
Fig. 1. Defective cholesterol clearance limits lesion regeneration in aged mice. (A) Images of corpus callosum lesions stained with fluoromyelin (green) and IBA1 (red) in 3 month old (3M), 12 month old (12M) and 12 month old mice treated with GW3965 (12M+GW3965) at 14 dpi. Scale bar, 100 µm. (B and C) Quantification of lesion area in mm$^2$ determined by luxol fast blue (LFB) and in mm$^3$ by fluoromyelin staining at 14 dpi. (D) Confocal images of 3M, 12M and 12M+GW3965 corpus callosum lesions showing IBA1 (red), fluoromyelin (green) and LAMP1 (cyan). Scale bar, 40µm. Magnified images of the boxed areas are show next to the images. (E) Change in number of IBA1$^+$ cells in corpus callosum lesions compared to contralateral unlesioned side. (F) Number of IBA1$^+$/fluoromyelin$^+$/LAMP1$^+$ cells in lesioned corpus callosum at 14 dpi. (G) Semithin section and (H) quantification of foam cells of 3M, 12M and 12M+GW3965 corpus callosum lesions. Scale bar, 10 µm. (I) Reflection microscopy images of spinal cord lesions, showing crystals (white) in lectin$^+$ phagocytes (red), and (J) relative quantification of the fluorescence intensity of the reflected light. Scale bar, 25 µm. (K to M) Quantitative PCR analysis of Apoe, Abca1 and Abcg1 in 4 dpi lesions of 3M and 12M mice. All data are mean ± SEM; *P < 0.05, **P < 0.01, ***P < 0.001 by one way ANOVA test, with Tukey's multiple comparison test.
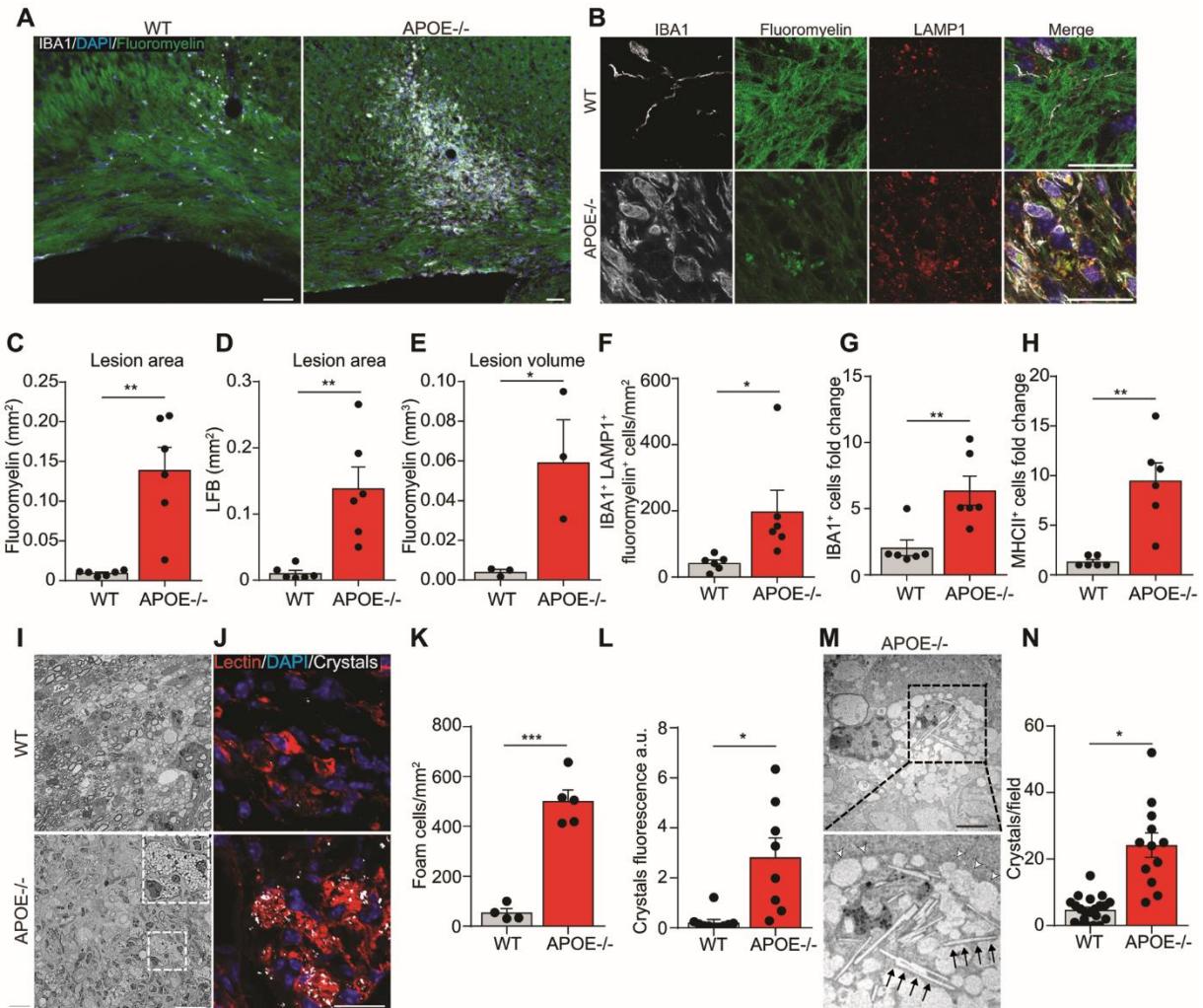
Fig. 2. APOE is required for cholesterol clearance in demyelinating lesions. (A and B) Images of corpus callosum lesions in WT and APOE−/− mice at 21 dpi showing fluoromyelin staining (green), IBA1 (white), DAPI (blue) and LAMP1 (red). (C and D) Quantification of lesion area in mm$^2$ at 21 dpi as determined by fluoromyelin and luxol fast blue (LFB) staining. (E) Lesion volume in mm$^3$ measured by fluoromyelin staining in consecutive sections. (F) Number of IBA1$^+$/fluoromyelin$^+$/LAMP1$^+$ cells per mm$^2$ in lesions at 21 dpi. (G and H) Change in the number of IBA1$^+$ and MHC II$^+$ cells in the lesioned corpus callosum as compared to the contralateral unlesioned side. (I) Representative images (boxed area shown at larger magnification in right corner) and (K) quantification of foam cells in spinal cord lesions in WT and APOE−/− mice at 21 dpi. (J) Reflection microscopy images of 21 dpi lysolecithin lesions, showing crystals (white) in lectin$^+$ phagocytes (red), and (L) relative quantification of the fluorescence intensity of the reflected light. (M) Transmission electron microscopy images of foam cells in 21 dpi lesions of APOE−/− mice (boxed area shown below at higher magnification), showing needle-like cholesterol crystals (black arrows) and lipid droplets (white arrowheads), and (N) relative quantification of crystals. All data are mean ± SEM; *P < 0.05, **P < 0.01, ***P < 0.001, two-tailed Student's t-test. Scale bars in (A, B, I, and J) are 25 μm; scale bar in (K) is 2.5 μm.
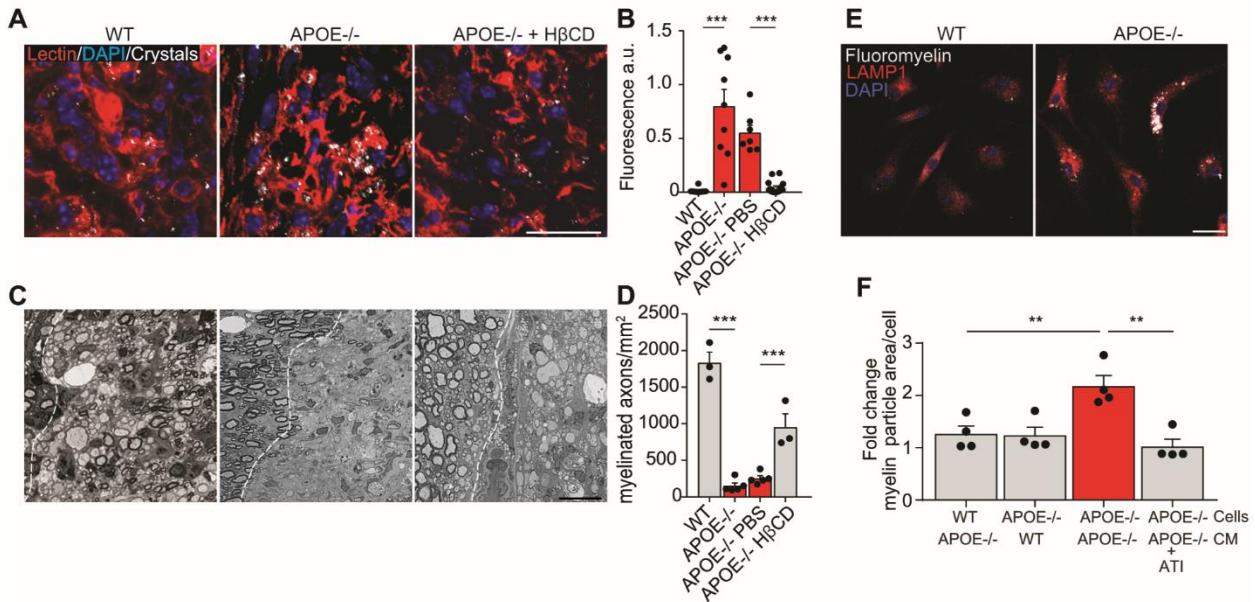
Fig. 3. Enhancing cholesterol clearance prevents lysosomal storage of myelin debris and crystal formation. (A) Representative images with crystals (white) and lectin⁺ phagocytes (red); and (B) quantification of cholesterol crystals in lysolecithin lesions of WT, APOE−/− and APOE−/− mice treated with HBCD or PBS. (C) Representative images of Methylenblue-Azur II staining and (D) quantification of remyelination in lysolecithin lesions at 21 dpi. The edges of the lesions are identified by a dashed line. (E) Confocal images of primary microglial cell cultures prepared from WT or APOE−/− mice, treated with myelin debris and stained for LAMP1 (red), fluoromyelin (white) and DAPI (dark blue) at 24 hours post-treatment. Microglia from WT or APOE−/− mice were treated with myelin debris and subsequently transferred in media conditioned (CM) either by WT or APOE−/− astrocytes. APOE−/− microglia cells in APOE−/− conditioned media were additionally treated with APOE mimetic peptide (ATI). (F) Change in the area of myelin particles per cell as compared to WT cells in WT conditioned media. All data are mean ± SEM; *P < 0.05, **P < 0.01, ***P < 0.001, by two way ANOVA, with Tukey's multiple comparison test. Scale bar is 25 μm in (A); scale bar is 100 μm in (B).
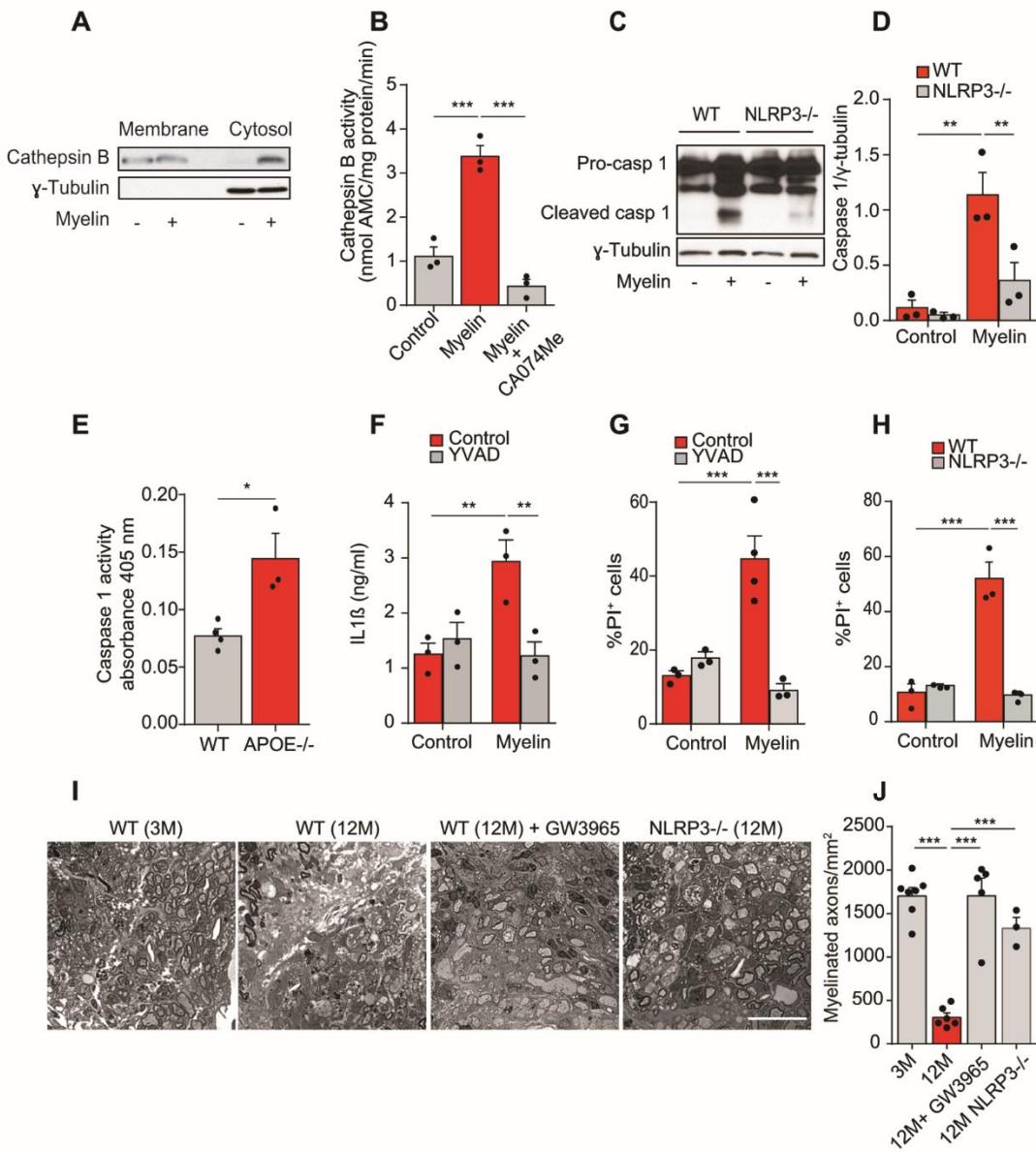
Fig. 4. **Defective myelin debris clearance activates the NLRP3 inflammasome.** (**A**) Immunoblot of cytosol and membrane fractions of primary bone marrow-derived macrophages (BMDM) 12 hours after treatment with myelin debris for cathepsin B and γ-tubulin. (**B**) Cathepsin B activity assay of the cytosolic fraction of control macrophages 12 hours after treatment with myelin debris in the presence or absence of the cathepsin B inhibitor, CA074me (10μM). (**C** and **D**) Immunoblot and quantification of the active subunit of caspase 1 (p20) after myelin debris treatment of WT or NLRP3−/− BMDM. The intensity of the p20 band was normalized to γ-tubulin. (**E**) Caspase 1 activity in lysates from lysolecithin lesions of WT and APOE−/− mice at 21 dpi. (**F**) ELISA for IL1β release in WT BMDM, after treatment with myelin debris with or without YVAD. (**G**) Quantification of the percentage of dead cells (propidium iodide positive, PI+) after myelin debris treatment (12 hours) in the presence or absence of caspase 1 inhibitor (YVAD). (**H**) Quantification of PI+ cells after treatment of WT and NLRP3−/− BMDM with myelin debris for 12 h. (**I**) Methylenblue-Azur II staining of remyelinating lesions in the spinal cord of 3M, 12M, GW3965 treated 12 M, and 12M old NLRP3−/− mice and (**J**) relative quantification of myelinated fibers. All data are mean ± SEM; *P < 0.05, **P < 0.01, ***P < 0.001 by one way ANOVA test, with Tukey's multiple comparison test and two-tailed Student's t-test (E). Scale bar, 25 μm.

# Science

## Defective cholesterol clearance limits remyelination in the aged central nervous system

Ludovico Cantuti-Castelvetri, Dirk Fitzner, Mar Bosch-Queralt, Marie-Theres Weil, Minhui Su, Paromita Sen, Torben Ruhwedel, Miso Mitkovski, George Trendelenburg, Dieter Lütjohann, Wiebke Möbius and Mikael Simons

| | |
|---|---|
| **ARTICLE TOOLS** | http://science.sciencemag.org/content/early/2018/01/03/science.aan4183 |
| **SUPPLEMENTARY MATERIALS** | http://science.sciencemag.org/content/suppl/2018/01/03/science.aan4183.DC1 |
| **REFERENCES** | This article cites 29 articles, 9 of which you can access for free<br>http://science.sciencemag.org/content/early/2018/01/03/science.aan4183#BIBL |
| **PERMISSIONS** | http://www.sciencemag.org/help/reprints-and-permissions |

Use of this article is subject to the Terms of Service